DØ Note 5438-CONF

Search for Scalar Top Admixture in the $t\bar{t}$ Lepton+Jets Final State at $\sqrt{s} = 1.96$ TeV in 1 fb^{-1} of DØ Data

The DØ Collaboration
URL http://www-d0.fnal.gov

(Dated: July 22, 2007)

A search has been performed for scalar top (stop) quark pair production in the lepton+jets channel in ≈ 1 fb^{-1} of data. Kinematic differences between the exotic $\tilde{t}_1\bar{\tilde{t}}_1$ and the dominant $t\bar{t}$ process are used to separate the two possible contributions. For stop (chargino) masses of 145–175 (105–135) GeV we obtain upper cross section limits at 95% confidence level for $\tilde{t}_1\bar{\tilde{t}}_1$ production that are a factor of $\approx$ 7–12 higher than expected for the Minimal Supersymmetric Standard Model (MSSM).

Preliminary Results for Summer 2007 Conferences

I. INTRODUCTION

Supersymmetry (SUSY) establishes a superpartner for each the left and the right-handed top quark [1]. Because of the large top quark mass the mixing between the superpartners of the left-handed and the right-handed top quark can be substantial. This provides a large difference in the mass eigenvalues of the scalar top quark ("stop quark") with the lighter stop quark $\tilde{t}_1$ possibly being the lightest scalar quark and well within reach at the Tevatron. An interesting reason for a light stop quark derives from electroweak baryogenesis, which is excluded in the Standard Model, but is feasible in a supersymmetric model when the stop quark is lighter than the top quark [2].

At the Tevatron stop quarks are produced mainly in diagonal pairs $\tilde{t}_1\bar{\tilde{t}}_1/\tilde{t}_2\bar{\tilde{t}}_2$ [3]. At lowest order in QCD the production processes are quark-antiquark annihilation or gluon fusion. Next-to-leading order (NLO) calculations exist and are even incorporated in tools such as PROSPINO, which provides NLO cross sections for supersymmetric particles [4]. The cross section depends primarily on the stop quark mass, although there is also a weak dependence on the gluino mass, the mixing angle and other squark masses arising from higher-order corrections. At a mass of 175 GeV, which is the approximate mass of the top quark, the cross section is 0.579 pb, about a tenth of the theoretical cross section for $t\bar{t}$ production for a top quark of the same mass, which at next-to-next-to-leading order is calculated to be 6.77 pb [5].

In this analysis, we consider stop quark masses equal to or lighter than the top quark mass, with the chargino and neutralino masses set close to their experimental lower limits. In this scenario the decays $\tilde{t}_1 \to b\tilde{\chi}_1^+$ and $\tilde{t}_1 \to bW^+\tilde{\chi}_1^0$ shown on the left in Figure 1 can be important. In the first case, the chargino $\tilde{\chi}_1^\pm$ decays to a W boson and a neutralino $\tilde{\chi}_1^0$ so that from this stage on the two decays become identical. The right plot in Figure 1 shows that this decay can dominate over a large range of $\tan\beta$.

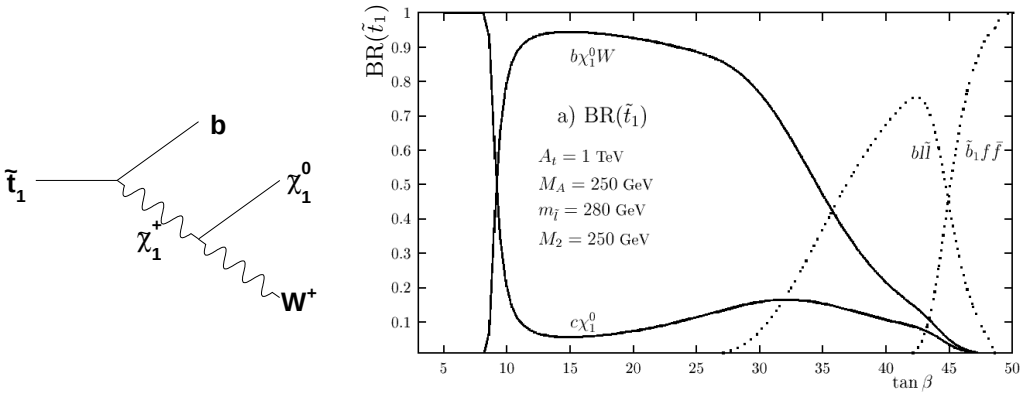

Figure 1: Left: Three-body decay considered in this anaysis. Right: Branching ratio for two-body and three-body decay modes of the lightest stop quark $\tilde{t}_1$ as a function of $\tan\beta$ [6]. The stop quark mass in this plot ranges from 170 GeV at $\tan\beta$=5 to 230 GeV at $\tan\beta$=45.

The subsequent decay of the W boson determines the event topology just as in top quark pair production ($t\bar{t}$) events. The resulting $\tilde{t}_1\bar{\tilde{t}}_1$ event signature is consequently very similar to the $t\bar{t}$ signature, thus making it possible for the $\tilde{t}_1\bar{\tilde{t}}_1$ signal to be contained in the $t\bar{t}$ event sample. For this analysis, we consider the decay channel with one W boson decaying to hadrons and the other one to leptons. It does not play a role whether the W boson is real or virtual, both scenarios will give the same signature. The resulting final state consists of one high-p_T lepton, missing transverse energy $\not\!\!E_T$ from the neutrino and the neutralinos, two b-jets, and two light quark jets. This will be referred to as lepton+jets channel.

The limits on masses of supersymmetric particles from LEP can be found in Reference [7]. In the MSSM with lowest order gaugino and sfermion mass unification at the GUT scale the limit on the lightest neutralino as the lightest supersymmetric particle (LSP) is 47 GeV. Charginos are excluded up to masses of 103.5 GeV, depending on the model. Stop quarks in the $\tilde{t}_1 \to c\tilde{\chi}_1^0$ and $\tilde{t}_1 \to b\ell^+\tilde{\nu}_\ell$ decay channels are excluded up to masses of 100 GeV. Limits on the stop quark mass have also been obtained at the Tevatron. In the $\tilde{t}_1 \to b\tilde{\chi}_1^+$ channel considered in this analysis, CDF obtained upper limits on the stop quark production cross section in Run I for stop quark masses between 100 and 120 GeV [8]. In Run II CDF sets a mass limit in the $\tilde{t}_1 \to c\tilde{\chi}_1^0$ channel at 132 GeV with 295 pb^{-1} of data [9],

DØ has a limit of 149 GeV for a neutralino mass of 63 GeV with 995 pb^{-1} in the same channel [10]. DØ also sets a limit in the $\tilde{t}_1 \to b\ell^+\tilde{\nu}_\ell$ channel of 186 GeV for a sneutrino mass of 71 GeV with 400 pb^{-1} of data [11].

II. DATA SAMPLE

The analyzed dataset comprises data collected by the DØ detector at a center-of-mass energy of 1.96 TeV between August 2002 and December 2005. This corresponds to an integrated luminosity of 913 pb^{-1} for the electron+jets channel with triggers requiring one electron with $p_T > 15$ GeV and at least one jet with p_T thresholds between 15 and 30 GeV, depending on the running period. For the muon+jets channel 871 pb^{-1} were collected with triggers requiring a muon and at least one jet with p_T thresholds between 20 and 35 GeV. It is the same dataset that was used to measure the $t\bar{t}$ cross section in the lepton+jets channel [12].

III. MONTE CARLO SIMULATION

The $\tilde{t}_1\bar{\tilde{t}}_1$ signal events in the lepton+jets topology were generated using PYTHIA v6.323 [13] in its general MSSM mode. The neutralino $\tilde{\chi}_1^0$ is the LSP and the MSSM parameters are chosen as follows:

- $\tan\beta = 20$, $\mu = 225$ GeV, $M_A = 800$ GeV, $M_1 = 53$ GeV, $M_3 = 500$ GeV,
- Trilinear couplings $A_b = A_\tau = 200$ GeV,
- Scalar lepton masses $M_{\tilde{l}_L} = M_{\tilde{l}_R} = M_{\tilde{\tau}_L} = M_{\tilde{\tau}_R} = 200$ GeV,
- Scalar quark masses $M_{\tilde{q}_L} = M_{\tilde{q}_R} = M_{\tilde{b}_R} = M_{\tilde{t}_R} = 250$ GeV.

For this set of SUSY parameters the branching ratio for $\tilde{t}_1 \to \tilde{\chi}_1^+ b$ is 100% according to PYTHIA. The masses of the stop quark, the lightest chargino, and the lightest neutralino are determined essentially by the top trilinear coupling A_t and the gaugino masses M_2 and M_1, respectively. These were chosen to produce the specific mass points given in Table I. The table also shows the corresponding cross section for $\tilde{t}_1\bar{\tilde{t}}_1$ production for each mass point as calculated in PROSPINO. The mass difference between the chargino and the neutralino determines if the chargino will decay to a neutralino and a real W boson or to a neutralino and a lepton with a neutrino or quarks via a virtual W boson. For the produced mass points a real W boson is only possible for the mass point with a chargino mass of 135 GeV (and a stop quark mass of 175 GeV).

Mass point	$\sigma_{\tilde{t}_1\bar{\tilde{t}}_1}$	A_t	$m_{\tilde{t}_1}$	M_2	$m_{\tilde{\chi}_1^\pm}$	M_1	$m_{\tilde{\chi}_1^0}$
Stop 175/135	0.579 pb	357 GeV	175 GeV	164 GeV	135 GeV	53 GeV	50 GeV
Stop 175/120	0.579 pb	357 GeV	175 GeV	144 GeV	120 GeV	53 GeV	50 GeV
Stop 175/105	0.579 pb	357 GeV	175 GeV	125 GeV	105 GeV	53 GeV	50 GeV
Stop 160/120	1.00 pb	387 GeV	160 GeV	144 GeV	120 GeV	53 GeV	50 GeV
Stop 160/105	1.00 pb	387 GeV	160 GeV	125 GeV	105 GeV	53 GeV	50 GeV
Stop 145/105	1.80 pb	414 GeV	146 GeV	125 GeV	105 GeV	53 GeV	50 GeV

Table I: Stop/Chargino mass points used in this analysis with their $\tilde{t}_1\bar{\tilde{t}}_1$ cross section, SUSY parameters and particle masses.

All background samples in this analysis are identical to those used in standard DØ $t\bar{t}$ analyses.The $t\bar{t}$ events were produced using PYTHIA for a top quark mass of 175 GeV. The W+jets samples were generated using ALPGEN [14] followed by PYTHIA for the fragmentation and hadronization of quarks and gluons. The production also included a jet-matching algorithm following the MLM prescription [15] to match parton showers generated by PYTHIA and avoid double counting. The W+jets samples consist of the subsamples Wjj, $Wc\bar{c}$,and $Wb\bar{b}$, where Wjj includes the Wcj subprocess. The Z+jets samples were generated using ALPGEN in the same way as the W+jets samples described above. $Z \to ee, \tau\tau, \nu\nu$ decays were considered in the electron+jets channel, and $Z \to \mu\mu, \tau\tau, \nu\nu$ in the muon+jets channel. Single top event samples were generated with the COMPHEP-SINGLETOP Monte Carlo event generator [16], which produces events whose kinematic distributions match those from NLO calculations. The top quark mass was assumed to be 175 GeV and PYTHIA was used to add the underlying event and initial and final state radiation. The

diboson samples WW, WZ, and ZZ were generated using PYTHIA. All samples passed through a full DØ-detector simulation using GEANT [17] and the events were reconstructed by the standard DØ reconstruction program.

IV. EVENT SELECTION

As described in Section I the lepton+jets final state of stop quark pair production and the subsequent decays is an isolated high-p_T lepton, large missing transverse energy $\not\!\!E_T$, two b-jets, and two light quark jets. The analysis is performed separately in two different channels, the results of which are combined in the end. The electron+jets (e+jets) channel considers the case where the lepton is an electron, and the muon+jets (μ+jets) channel considers the muon. The preselection selects events corresponding to the described event signature.

For the e+jets channel the requirements are:

- At least four jets with $p_T > 15$ GeV and pseudorapidity (relative to the center of the detector) $|\eta_{det}| < 2.5$
- Highest-p_T jet with $p_T > 40$ GeV
- One isolated electron with $p_T > 20$ GeV and $|\eta_{det}| < 1.1$ originating from the primary vertex
- No second electron with $p_T > 15$ GeV and $|\eta_{det}| < 2.5$, no isolated muon with $p_T > 15$ GeV
- Good quality primary vertex with $|z_{PV}| \leq 60\ cm$ with at least three tracks
- $\not\!\!E_T > 20$ GeV and $\Delta\phi(e, \not\!\!E_T) > 0.7 \cdot \pi - 0.045 \cdot \not\!\!E_T$

For the μ+jets channel the requirements are:

- At least four jets with $p_T > 15$ GeV and pseudorapidity (relative to the center of the detector) $|\eta_{det}| < 2.5$
- Highest-p_T jet with $p_T > 40$ GeV
- One isolated muon with $p_T > 20$ GeV and $|\eta_{det}| < 2.0$ originating from the primary vertex
- No additional muon with invariant mass 70 $GeV < m_{\mu\mu} <$ 110 GeV with the selected muon (to reject $(Z \rightarrow \mu\mu) + jets$ events)
- No second muon with $p_T > 15$ GeV, no electron with $p_T > 15$ GeV
- Good quality primary vertex with $|z_{PV}| \leq 60\ cm$ with at least three tracks
- $\not\!\!E_T > 25$ GeV and $\Delta\phi(\mu, \not\!\!E_T) > 2.1 - 0.035 \cdot \not\!\!E_T$

Since the signal event signature contains two b-jets in the final state, a neural network b-jet tagging algorithm is used to identify the jets originating from b-quarks and we define the additional requirement:

- At least one jet tagged by the neural network b-tagging algorithm at working point "tight"

Later in the analysis it turns out to be useful to reconstruct the events to a $t\bar{t}$ hypothesis using a kinematic fitter called HITFIT, which is why we also require:

- Convergence of HITFIT

In the latter, the HITFIT algorithm fits events to a $t\bar{t}$ hypothesis by minimizing a χ^2 statistics within the constraints that both W boson masses are 80.4 GeV and that the masses of the two supposed reconstructed top quarks are the same [18]. The momenta of the detected objects are varied within their resolutions and b-tagging information is taken into account to reduce combinatorics.

Table II shows the total preselection efficiency as well as the number of expected signal events for each signal mass point. The total preselection efficiency is measured on $\tilde{t}_1\bar{\tilde{t}}_1$ events with respect to $\tilde{t}_1\bar{\tilde{t}}_1 \rightarrow b\bar{b}\tilde{\chi}_1^0\tilde{\chi}_1^0\ell\nu_\ell q\bar{q}'$, where ℓ can be an electron or muon from the decay of a W boson (or chargino), including the case where the W boson (or chargino) decays to a τ lepton first. Trigger efficiencies are included as well as corrections to agree with efficiencies measured using collider data.

Sample	e+jets		μ+jets	
	Efficiency	Expected Events	Efficiency	Expected Events
Stop 175/135	4.43 ± 0.10	4.0 ± 0.1	3.57 ± 0.08	3.1 ± 0.1
Stop 175/120	3.72 ± 0.10	3.1 ± 0.1	2.90 ± 0.09	2.3 ± 0.1
Stop 175/105	3.20 ± 0.10	2.8 ± 0.1	2.44 ± 0.09	2.0 ± 0.1
Stop 160/120	2.51 ± 0.08	3.6 ± 0.1	1.78 ± 0.06	2.4 ± 0.1
Stop 160/105	2.52 ± 0.08	3.8 ± 0.1	1.89 ± 0.06	2.7 ± 0.1
Stop 145/105	1.64 ± 0.06	4.5 ± 0.2	1.16 ± 0.05	3.0 ± 0.1

Table II: Preselection efficiencies in percent and expected number of $\tilde{t}_1\bar{\tilde{t}}_1$ signal events for a dataset of 913 pb^{-1} in the e+jets channel and 871 pb^{-1} in the μ+jets channel for all signal mass points. Only statistical uncertainties are included.

V. BACKGROUND ESTIMATION

The background sources in this analysis are identical to the ones in $t\bar{t}$ lepton+jets analyses, $t\bar{t}$ itself being the dominant one. They can be subdivided into two components, the instrumental background and the physics background.

The instrumental background is strong multijet production, where $\not\!\!E_T$ is created by mismeasurements and an electron may be faked by an electromagnetic jet or by a photon that converts in the detector material. A muon can arise from a semi-leptonic b-decay. The multijet background is estimated using collider data by exploiting the fact that it contains fake leptons, whereas the signal and physics background processes have a real isolated lepton. Details about the method are described in Reference [12].

The physics background consists of various physics processes, which can all result in the same final state as the signal, namely $t\bar{t}$ production, W+jets production, Z+jets production, single top production, and diboson production. The latter three are minor background sources and are estimated using their theoretical cross section. The procedure to separate $\tilde{t}_1\bar{\tilde{t}}_1$ events from $t\bar{t}$ events is described in Section VI.

The W+jets background is estimated using data before b-tagging by subtracting the multijet background and all other background sources as determined by their theoretical cross section, including the $t\bar{t}$ background, from the data. The W+jets contribution is then scaled by a normalization factor α_W to fill in the rest. The heavy flavor samples get a higher relative contribution by the factor of $k_{HF} = 1.17 \pm 0.18$ [21]:

$$\begin{aligned} N_{W+jets} &= N_{Wjj} + N_{Wc\bar{c}} + N_{Wb\bar{b}} && (1)\\ &= \alpha_W \cdot (\hat{N}_{Wjj} + k_{HF}\hat{N}_{Wc\bar{c}} + k_{HF}\hat{N}_{Wb\bar{b}}) && (2)\\ &= N_{data} - N_{multijet} - N_{t\bar{t}} - N_{Z+jets} - N_{singletop} - N_{diboson}, && (3) \end{aligned}$$

where $\hat{N}_{Wxx}$ is the number of W+jets events before being normalized and N_{Wxx} after. Using (2) and (3) before b-tagging, α_W is determined separately for each jet bin. The result is shown together with the event yields before b-tagging in Table III. After b-tagging and convergence of HITFIT this α_W is then applied in (2) to obtain the yields in (1). When normalizing the W+jets background by this procedure, no signal contribution is assumed. The yields after b-tagging are shown in Table IV. Alongside the yields in the four jet multiplicity bins another column with the yields in the fourth jet bin after the convergence of the kinematic fitter HITFIT is shown. Control plots showing the data-MC agreement can be found in Appendix A.

VI. SIGNAL EXTRACTION

A. Likelihood Discriminant

Because of the similarity of the $\tilde{t}_1\bar{\tilde{t}}_1$ and $t\bar{t}$ final states a multivariate technique is employed. We therefore study the kinematic differences between $\tilde{t}_1\bar{\tilde{t}}_1$ and $t\bar{t}$ events and combine them into a likelihood discriminant for signal-background separation. For each stop quark mass point an optimal set of variables is chosen based on their discrimination power and correlation.

By comparing the value x_i of a variable in a given event to the distribution of that variable in the $\tilde{t}_1\bar{\tilde{t}}_1$ signal and in the $t\bar{t}$ background, a probability to be signal $P_{sig}(x_i)$ and a probability to be background $P_{bg}(x_i)$ can be assigned

Sample	e+jets				μ+jets			
	=1 jet	=2 jets	=3 jets	≥4 jets	=1 jet	=2 jets	=3 jets	≥4 jets
α_W	1.42	1.46	1.32	0.86	1.48	1.60	1.62	1.25
$N_{t\bar{t}}$	11.6	71.5	131.9	170.0	7.1	48.3	95.7	137.1
$N_{Wb\bar{b}}$	248.3	226.1	84.2	22.2	190.1	204.7	84.7	28.0
$N_{Wc\bar{c}}$	764.6	630.4	211.4	45.5	610.8	548.8	219.8	57.2
N_{Wjj}	11702.8	4974.1	1102.4	211.4	9754.8	4456.9	1143.1	263.7
N_{Z+jets}	238.2	277.2	120.9	50.0	847.6	446.1	160.7	63.2
$N_{singletop}$	13.2	39.0	17.5	6.2	9.4	30.0	13.7	4.8
$N_{diboson}$	95.0	201.0	65.7	18.1	71.1	169.1	55.1	15.3
$N_{multijet}$	506.4	754.8	375.0	139.6	114.2	148.0	65.4	24.6
N_{SUM}	13580	7174	2109	663	11605	6052	1838	594
N_{data}	13580	7174	2109	663	11605	6052	1838	594

Table III: W+jets normalization factor α_W and background and data yields before b-tagging for events with =1,=2,=3, and ≥4 jets.

Sample	e+jets					μ+jets				
	=1 jet	=2 jets	=3 jets	≥4 jets	HITFIT	=1 jet	=2 jets	=3 jets	≥4 jets	HITFIT
α_W	1.42	1.46	1.32	0.86	0.86	1.48	1.60	1.62	1.25	1.25
$N_{t\bar{t}}$	4.9	39.3	77.6	108.3	103.0	3.1	27.8	58.5	89.8	84.2
$N_{Wb\bar{b}}$	70.6	86.0	35.4	9.1	8.5	56.5	79.8	36.1	12.2	11.1
$N_{Wc\bar{c}}$	39.5	46.8	20.1	5.0	4.8	27.2	39.6	22.2	6.9	6.5
N_{Wjj}	124.5	59.0	13.2	4.0	3.8	89.0	51.3	19.3	4.4	4.0
N_{Z+jets}	2.9	7.5	5.2	3.0	2.8	14.3	14.8	6.9	3.9	3.3
$N_{singletop}$	5.1	19.3	9.3	3.6	3.1	3.7	15.2	7.5	2.9	2.5
$N_{diboson}$	3.1	11.6	4.2	1.4	1.4	2.8	10.2	3.8	1.4	1.2
$N_{multijet}$	16.2	41.1	22.3	11.1	10.7	6.6	12.0	3.0	2.9	3.2
N_{SUM}	266.8	310.7	187.2	145.6	138.1	203.1	250.7	157.5	124.3	116.0
N_{data}	255	329	193	145	133	189	265	163	146	135

Table IV: W+jets normalization factor α_W and background and data yields after b-tagging for events with =1,=2,=3, and ≥4 jets and events with ≥4 jets for which the kinematic fitter HITFIT converged.

to the event. Assuming no correlations at all, the individual probabilities for each variable can be multiplied to give an overall probability for the event:

$$P_{sig/bg}(\mathbf{x}) = \prod_i P_{sig/bg}(x_i), \tag{4}$$

where $\mathbf{x} = (x_1, x_2, ...)$ is the collection of all variable values in this event. These probabilities are then used to build the likelihood discriminant $\mathcal{L}(\mathbf{x})$:

$$\mathcal{L}(\mathbf{x}) = \frac{P_{sig}(\mathbf{x})}{P_{sig}(\mathbf{x}) + P_{bg}(\mathbf{x})}. \tag{5}$$

For signal-like events $\mathcal{L}(\mathbf{x})$ tends toward 1, whereas for background-like events it tends to 0. Full samples are used to build the templates and the likelihood discriminant for each sample to minimize the statistical uncertainty.

Depending on the stop quark mass point a subset of the following eleven variables was used. The term "leading jet" refers to the highest-p_T jet in the event:

- The p_T **of the leading b-tagged jet** $p_T(\mathbf{b}{-}jet)$ differs in $\tilde{t}_1\bar{\tilde{t}}_1$ and $t\bar{t}$ events because of the different masses of the W-boson that the top quark decays to and the chargino, that the stop quark decays to. Since the chargino is heavier, it leaves less phase space for the b-quark and the b-jet spectrum is lower.
- The W **transverse mass** $M_T(W)$ is reconstructed by using the kinematic information of the lepton and $\not\!\!E_T$ in the event. Most stop quark mass points do not have a real W-boson present and thus this quantity reconstructs to a lower mass.

- $K_{Tmin} = \Delta R_{jj}^{min} E_T^{min}$ provides a measure of the minimum jet p_T relative to another. Only the four highest-p_T jets are considered in the definition. ΔR_{jj}^{min} is the minimum ΔR distance between a pair of jets and E_T^{min} is the transverse energy of the lesser jet of that pair. For mass points where the $\tilde{t}_1\bar{\tilde{t}}_1$ events have a virtual W boson, the quarks originating from that virtual W boson have lower p_T compared to quarks from a real W boson and the ΔR distance between them is small.

For the definition of the following quantities all jets except the leading b-tagged jet are ordered by p_T. The three highest-p_T ones are denoted "leading other jet", jet 3 and jet 4.

- The **invariant mass of the system of jet 3 and jet 4** $m(j,j)$. In the case of $t\bar{t}$ events these two jets are often the light jets in the event and this quantity reproduces the hadronic W-boson mass. For $\tilde{t}_1\bar{\tilde{t}}_1$ events it reconstructs a lower mass even for the mass point with a real W-boson.
- The distance in $\eta - \varphi$ space ΔR **between the leading b-tagged jet and the leading other jet** $\Delta R(b, lead)$. This and the following variable are derived from the ΔR between the W-boson and the b-quark from the same top or stop quark, which in $\tilde{t}_1\bar{\tilde{t}}_1$ events is much smaller than in $t\bar{t}$ events.
- ΔR **between the lepton and the leading b-tagged jet** $\Delta R(lep, b)$ shows the same kind of separation as the last variable.

The last variables are provided by the kinematic fitter HITFIT, which reconstructs events to a $t\bar{t}$ hypothesis as described in Section IV. Because it cannot take the neutralinos in to account, HITFIT fails to reconstruct stop quark events correctly, which is evident when comparing the HITFIT results with the Monte Carlo truth distributions. But that fact is unimportant, since it still converges on a large fraction of the signal events and is used to identify and separate the $t\bar{t}$ background from the $\tilde{t}_1\bar{\tilde{t}}_1$ signal:

- The **top mass as reconstructed by** HITFIT m_t^{hf} gives a lower mass for $\tilde{t}_1\bar{\tilde{t}}_1$ events, not only because the stop quark mass is often lower, but also because energy is carried away by the neutralinos, which are not considered in this reconstruction.
- The quantity $\cos\theta^*(b,b)^{hf}$ is reconstructed using the b-jets and their kinematics as determined by HITFIT. θ^* is the angle of the b-jet from the hadronic top or stop quark to the beam axis in the center of mass system of the two b-jets. It is a good approximation of $\cos\theta^*(t,t)$, where t are the top quarks or the stop quarks, whose separation is a direct consequence of the different spins. The preselection washes out the separation and HITFIT is not meant to reconstruct stop quark events, which is why this variable is used instead.
- The **invariant mass between the b-jets** $m^{hf}(b,b)$ is reconstructed using the assignments and kinematics by HITFIT.
- As mentioned before the ΔR between the correct pair of W-boson and b-quark gives good separation. In HITFIT the assignment is not always correct in $\tilde{t}_1\bar{\tilde{t}}_1$ events, which is why for some mass points ΔR **between the correct** HITFIT **pair of hadronic W-boson and b-jet** $\Delta R(W,b)^{hf}_{corr}$ gives better separation,
- but for other mass points the ΔR **between the wrong** HITFIT **pair of hadronic W-boson and b-jet** $\Delta R(W,b)^{hf}_{wrong}$ gives better separation.

Table V summarizes which variables are used for which mass point. As an example, the top mass as reconstructed by HITFIT in the μ+jets channel is shown in Figure 2. On the left is a comparison of the distribution in the $\tilde{t}_1\bar{\tilde{t}}_1$ signal for the mass point 175/135 to the $t\bar{t}$ and W+jets background samples, on the right the data-MC agreement of this variable without any signal contribution in the signal jet bin of ≥ 4 jets after b-tagging and convergence of HITFIT. Figure 3 shows the resulting likelihood discriminant for the mass point 175/135 as a comparison between $t\bar{t}$ and signal as well as a comparison between the prediction and the data. Plots of the likelihood discriminant and all the input variables for the mass point 175/135 for both the e+jets and μ+jets channel can be found in Appendix B.

$m_{\tilde{t}_1}$	$m_{\tilde{\chi}_1^\pm}$	Variables in Likelihood Discriminant
175 GeV	135 GeV	$p_T(b\text{-jet})$, $\Delta R(b, lead)$, m_t^{hf}, $\cos\theta^*(b,b)^{hf}$
175 GeV	120 GeV	$p_T(b\text{-jet})$, $m(j,j)$, m_t^{hf}, $\Delta R(W,b)^{hf}_{wrong}$
175 GeV	105 GeV	$M_T(W)$, $m(j,j)$, K_{Tmin}, m_t^{hf}, $m^{hf}(b,b)$
160 GeV	120 GeV	$p_T(b\text{-jet})$, $m(j,j)$, m_t^{hf}, $\Delta R(W,b)^{hf}_{corr}$
160 GeV	105 GeV	$p_T(b\text{-jet})$, $M_T(W)$, $m(j,j)$, $\Delta R(lep,b)$, m_t^{hf}
145 GeV	105 GeV	$p_T(b\text{-jet})$, $M_T(W)$, $m(j,j)$, $\Delta R(lep,b)$, m_t^{hf}

Table V: Variables used in the likelihood discriminant for the different stop quark mass points.

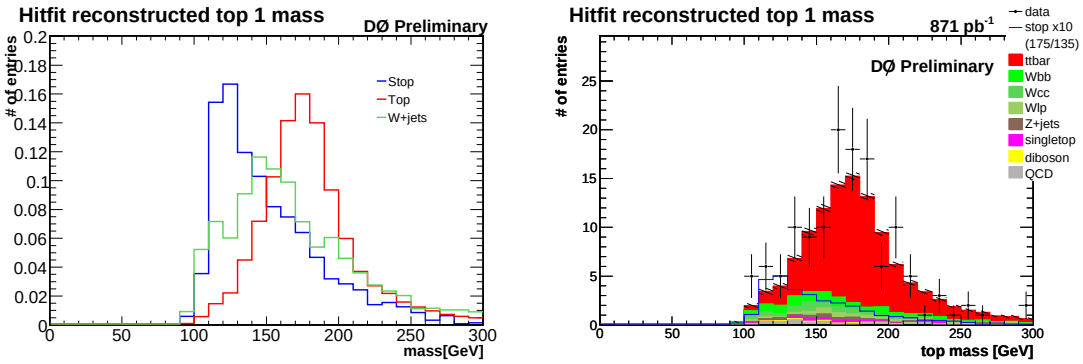

Figure 2: Top mass as reconstructed by HITFIT in the μ+jets channel. In the data-MC comparison on the right the distribution for the 175/135 mass point is overlaid ten times enhanced.

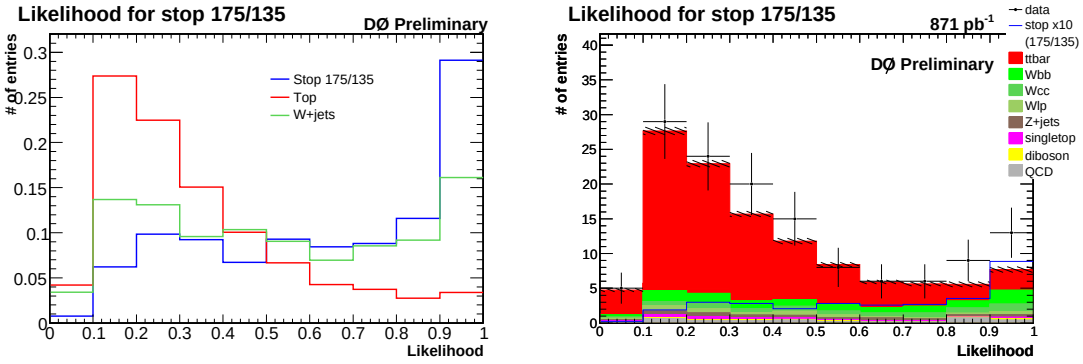

Figure 3: Likelihood discriminant for the 175/135 mass point in the μ+jets channel. In the data-MC comparison on the right the distribution for the 175/135 mass point is overlaid ten times enhanced.

B. Limit Setting Procedure

We use a Bayesian approach to extract limits from the likelihood discriminant distributions [19]. Under the assumption of a Poisson distribution for observed counts a binned probability function is formed. It is a product over all bins of the likelihood discriminant distribution and can be extended to combine the e+jets and μ+jets channels. For the signal cross section we assume a flat nonnegative prior probability. By integrating over the signal acceptances, background yields and integrated luminosity with Gaussian priors for each systematic uncertainty we obtain the posterior probability density as a function of the signal cross section. The limit at 95% confidence level is the point where the integral over the posterior probability density reaches 95% of its total. A measurement of the cross section is given by the maximum of the posterior probability density. In addition, the posterior probability can also be calculated as a function of two signal cross sections, so that a limit without the assumption of the $t\bar{t}$ theoretical cross section can be extracted with a simultaneous measurement of the $t\bar{t}$ cross section. The latter method is used as

a cross-check.

The expected results are derived on the sum of all preselected background Monte Carlo samples without a $\tilde{t}_1\bar{\tilde{t}}_1$ contribution, but including the $t\bar{t}$ contribution according to its theoretical value. They are shown in Table VI for the standard method, which assumes a $t\bar{t}$ cross section of 6.77 pb, and in Table VII for the cross-check method.

Sample	e+jets	μ+jets	combined
Stop 175/135	4.36 pb	5.36 pb	3.28 pb
Stop 175/120	6.36 pb	7.72 pb	4.97 pb
Stop 175/105	6.85 pb	7.55 pb	5.16 pb
Stop 160/120	6.79 pb	9.10 pb	5.42 pb
Stop 160/105	6.89 pb	10.26 pb	5.63 pb
Stop 145/105	9.30 pb	11.84 pb	7.27 pb

Table VI: Expected Bayesian limits at 95% confidence level on the $\tilde{t}_1\bar{\tilde{t}}_1$ cross section with systematic uncertainties.

Sample	$\tilde{t}_1\bar{\tilde{t}}_1$ limit			$t\bar{t}$ cross section		
	e+jets	μ+jets	combined	e+jets	μ+jets	combined
Stop 175/135	4.48 pb	5.56 pb	3.27 pb	$6.41^{+1.42}_{-1.20}$ pb	$6.55^{+1.63}_{-1.34}$ pb	$6.56^{+1.17}_{-1.05}$ pb
Stop 175/120	6.70 pb	8.20 pb	5.21 pb	$6.16^{+1.43}_{-1.25}$ pb	$6.20^{+1.64}_{-1.37}$ pb	$6.34^{+1.19}_{-1.06}$ pb
Stop 175/105	7.45 pb	7.96 pb	5.42 pb	$6.12^{+1.46}_{-1.25}$ pb	$6.16^{+1.66}_{-1.35}$ pb	$6.30^{+1.19}_{-1.05}$ pb
Stop 160/120	6.89 pb	9.38 pb	5.50 pb	$6.50^{+1.39}_{-1.24}$ pb	$6.38^{+1.68}_{-1.35}$ pb	$6.56^{+1.19}_{-1.04}$ pb
Stop 160/105	7.10 pb	10.79 pb	5.80 pb	$6.31^{+1.42}_{-1.21}$ pb	$6.32^{+1.75}_{-1.40}$ pb	$6.45^{+1.21}_{-1.05}$ pb
Stop 145/105	9.42 pb	12.19 pb	7.36 pb	$6.50^{+1.39}_{-1.22}$ pb	$6.52^{+1.69}_{-1.34}$ pb	$6.64^{+1.15}_{-1.03}$ pb

Table VII: Expected Bayesian limits at 95% confidence level on the $\tilde{t}_1\bar{\tilde{t}}_1$ cross section and expected $t\bar{t}$ cross section with systematic uncertainties obtained with the cross-check method.

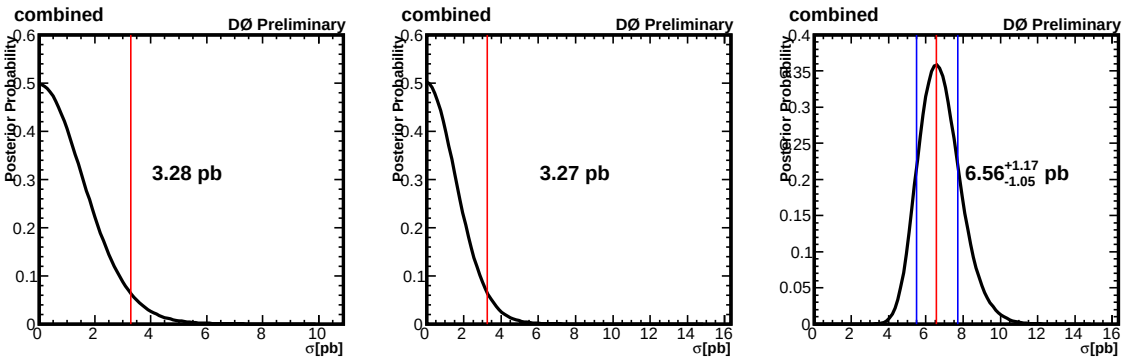

Figure 4: Expected posterior probabilities for the 175/135 mass point for e+jets and μ+jets channel combined. Left: as a function of the $\tilde{t}_1\bar{\tilde{t}}_1$ cross section obtained with the standard method, middle: as a function of the $\tilde{t}_1\bar{\tilde{t}}_1$ cross section obtained with the cross-check method, right: as a function of the $t\bar{t}$ cross section obtained with the cross-check method.

VII. SYSTEMATIC UNCERTAINTIES

There are two ways in which systematic uncertainties can enter the limit, one is by changing the expected event yield and the other by changing the shape of the likelihood discriminant distribution in addition. Table VIII summarizes the systematic uncertainties that only affect the yields. The uncertainties on the jet energy, the W+heavy flavor fraction in the W+jets background model and the modeling of the b-tagging also change the shape of the likelihood discriminant distribution.

Source	e+jets	μ+jets
Luminosity [20]	6.1%	6.1%
Monte Carlo Cross Section $t\bar{t}$	18.0%	18.0%
Monte Carlo Cross Section single top	12.6%	12.6%
Monte Carlo Cross Section Z+jets	15.0%	15.0%
Monte Carlo Cross Section diboson	6.8%	6.8%
Top Quark Mass	4.9%	4.2%
Multijet Background Estimation	21.1%	54.2%
W+jets Background Normalization	70.3%	30.1%
Primary Vertex	2.0%	2.0%
Lepton	5.5%	7.4%
Trigger	1.2%	2.7%

Table VIII: Summary of systematic uncertainties affecting the yield and $\pm 1\sigma$ variation taken to determine their effect.

VIII. RESULT

Table IX shows the measured limits at 95% confidence level for all mass points and in all channels and compares them to the theoretical cross sections. The result is also illustrated in Figure 5. Table X and Figure 6 show the same for the cross-check method, which gives consistent results. At this point we cannot exclude any of the stop masses, all observed limits are a factor of ≈7-12 above the theoretical predictions. In particular there is a fluctuation to higher values in the μ+jets channel, because there are more observed than expected events and the distributions in data and Monte Carlo do not agree as well as in the e+jets channel. One exception is the mass point 175/105, which is the only mass point that does not use the p_T of the leading b-tagged jet as input in its likelihood discriminant. This variable has a poorer data-MC agreement than other variables, but provides very good separation for almost all the mass points.

Sample	theoretical	e+jets	μ+jets	combined
Stop 175/135	0.579 pb	5.11 pb	10.20 pb	5.57 pb
Stop 175/120	0.579 pb	6.11 pb	12.41 pb	6.58 pb
Stop 175/105	0.579 pb	6.10 pb	9.28 pb	5.55 pb
Stop 160/120	1.00 pb	6.49 pb	15.79 pb	7.45 pb
Stop 160/105	1.00 pb	7.78 pb	20.75 pb	9.71 pb
Stop 145/105	1.80 pb	10.60 pb	24.21 pb	12.32 pb

Table IX: Observed Bayesian limits at 95% confidence level on the $\tilde{t}_1\bar{\tilde{t}}_1$ cross section with systematic uncertainties.

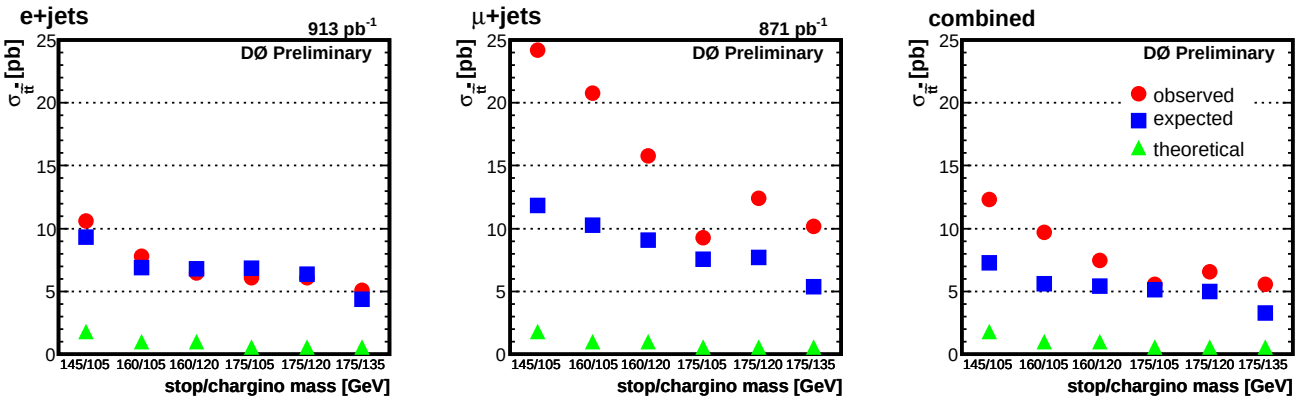

Figure 5: Observed and expected Bayesian limits at 95% confidence level on the $\tilde{t}_1\bar{\tilde{t}}_1$ cross section and theoretical cross section for $\tilde{t}_1\bar{\tilde{t}}_1$ at each mass point.

Sample	theoretical	$\tilde{t}_1\bar{\tilde{t}}_1$ limit			$t\bar{t}$ cross section		
	$\sigma_{\tilde{t}_1\bar{\tilde{t}}_1}$	e+jets	μ+jets	combined	e+jets	μ+jets	combined
Stop 175/135	0.579 pb	5.29 pb	10.72 pb	5.59 pb	$5.84^{+1.40}_{-1.17}$ pb	$6.96^{+1.83}_{-1.47}$ pb	$6.36^{+1.23}_{-1.04}$ pb
Stop 175/120	0.579 pb	6.57 pb	12.80 pb	6.90 pb	$5.93^{+1.36}_{-1.18}$ pb	$6.68^{+1.84}_{-1.55}$ pb	$6.45^{+1.22}_{-1.09}$ pb
Stop 175/105	0.579 pb	6.69 pb	9.46 pb	5.64 pb	$5.82^{+1.34}_{-1.15}$ pb	$6.92^{+1.92}_{-1.48}$ pb	$6.14^{+1.16}_{-1.02}$ pb
Stop 160/120	1.00 pb	6.63 pb	16.22 pb	7.64 pb	$6.12^{+1.34}_{-1.18}$ pb	$6.75^{+1.80}_{-1.49}$ pb	$6.51^{+1.20}_{-1.03}$ pb
Stop 160/105	1.00 pb	8.06 pb	21.96 pb	9.98 pb	$5.75^{+1.31}_{-1.13}$ pb	$5.99^{+1.81}_{-1.48}$ pb	$6.01^{+1.16}_{-0.97}$ pb
Stop 145/105	1.80 pb	10.81 pb	24.37 pb	12.56 pb	$5.98^{+1.34}_{-1.16}$ pb	$6.74^{+1.78}_{-1.46}$ pb	$6.46^{+1.20}_{-1.01}$ pb

Table X: Observed Bayesian limits at 95% confidence level on the $\tilde{t}_1\bar{\tilde{t}}_1$ cross section and measured $t\bar{t}$ cross section with systematic uncertainties obtained with the cross-check method.

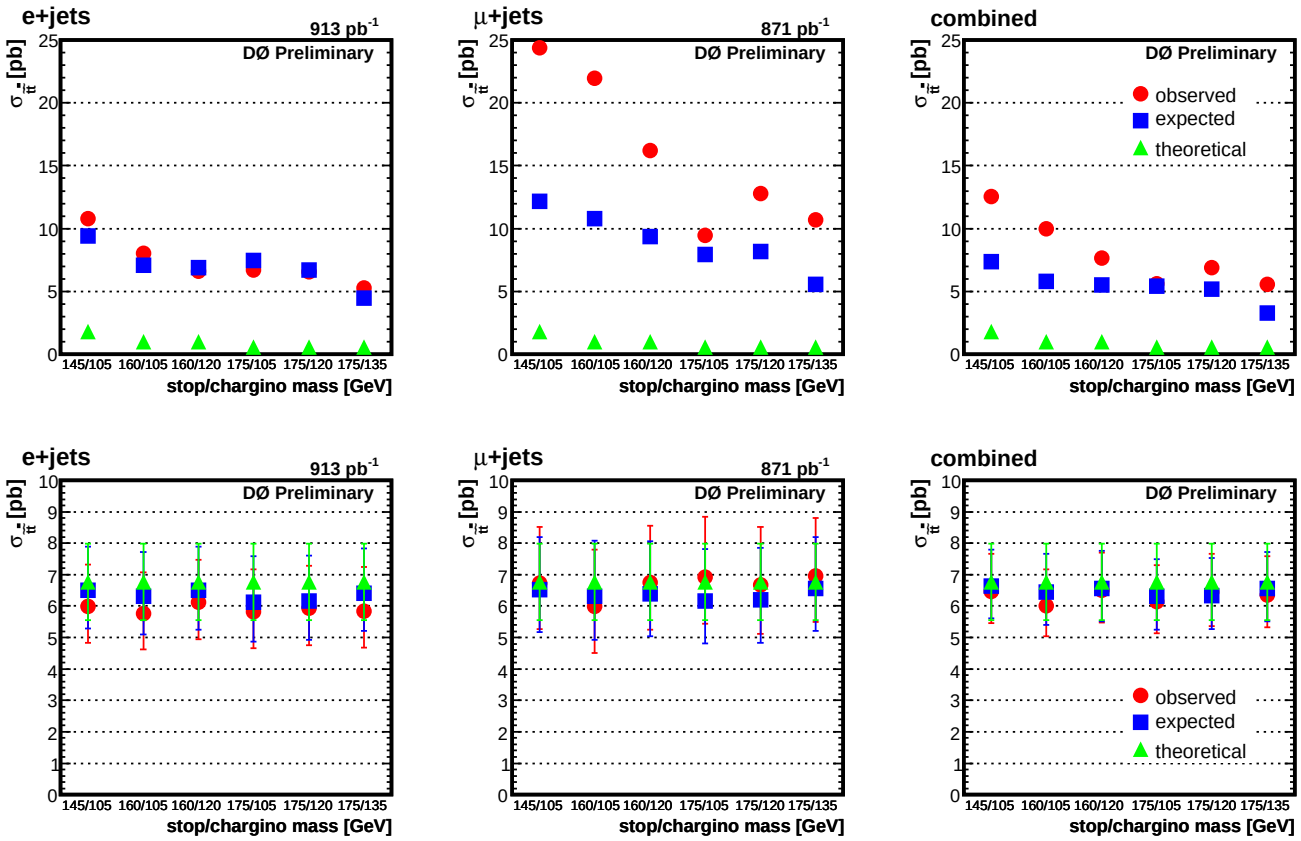

Figure 6: Top: Observed and expected Bayesian limits at 95% confidence level on the $\tilde{t}_1\bar{\tilde{t}}_1$ cross section and theoretical cross section for $\tilde{t}_1\bar{\tilde{t}}_1$ at each mass point obtained with the cross-check method. Bottom: Observed, expected and theoretical cross section for $t\bar{t}$.

Acknowledgments

We thank the staffs at Fermilab and collaborating institutions, and acknowledge support from the DOE and NSF (USA); CEA and CNRS/IN2P3 (France); FASI, Rosatom and RFBR (Russia); CAPES, CNPq, FAPERJ, FAPESP and FUNDUNESP (Brazil); DAE and DST (India); Colciencias (Colombia); CONACyT (Mexico); KRF and KOSEF (Korea); CONICET and UBACyT (Argentina); FOM (The Netherlands); Science and Technology Facilities Council (United Kingdom); MSMT and GACR (Czech Republic); CRC Program, CFI, NSERC and WestGrid Project (Canada); BMBF and DFG (Germany); SFI (Ireland); The Swedish Research Council (Sweden); CAS and CNSF

(China); Alexander von Humboldt Foundation; and the Marie Curie Program.

---

[1] H. Baer, X. Tata, *Weak Scale Supersymmetry: From Superfields to Scattering Events*, Cambridge University Press (2006).

[2] M. Carena, M. Quiros, C.E.M. Wagner, *Opening the Window for Electroweak Baryogenesis*, Phys. Lett. **B380**, 81 (1996). M. Carena, M. Quiros, C.E.M. Wagner, *Electroweak baryogenesis and Higgs and stop searches at LEP and the Tevatron*, Nucl. Phys. **B524**, 3 (1998).

[3] W. Beenakker *et al.*, *Stop Production at Hadron Colliders*, Nucl. Phys. B515 (1998) 3-14.

[4] W. Beenakker *et al.*, *PROSPINO: A Program for the Production of Supersymmetric Particles in Next-to-leading Order QCD*, arXiv:hep-ph/9611232v1 (1996).
PROSPINO homepage `http://www.ph.ed.ac.uk/~tplehn/prospino/`.

[5] N. Kidonakis, R. Vogt, *Next-to-next-to-leading order soft-gluon corrections in top quark hadroproduction*, Phys. Rev. D **68**, 114014 (2003).

[6] C. Boehm, A. Djouadi, Y. Mambrini, *Decays of the lightest top squark*, Phys. Rev. D **61**, 095006 (2000).
A. Djouadi, Y. Mambrini, *Three-body decays of top and bottom squarks*, Phys. Rev. D **63**, 115005 (2001).

[7] LEPSUSYWG, ALEPH, DELPHI, L3 and OPAL experiments, note LEPSUSYWG/07-05 (`http://lepsusy.web.cern.ch/lepsusy/Welcome.html`).

[8] A.A. Affolder *et al.* (CDF Collaboration), *Search for scalar top quark production in $p\bar{p}$ collisions at $\sqrt{s}$=1.8 TeV*, Phys. Rev. Lett. **84**, 5273 (2000).

[9] CDF Collaboration, *Search for Direct Pair Production of Scalar Top and Scalar Bottom Quarks in $p\bar{p}$ Collisions at $\sqrt{s}$=1.96 TeV*, CDF Note 8411 (2006). (`http://www-cdf.fnal.gov/physics/exotic/r2a/20060622.stopsbottom/`)

[10] DØ Collaboration, *Search for the pair production of scalar top quarks in acoplanar charm jet + Missing transverse energy final state in $p\bar{p}$ collisions at $\sqrt{s}$=1.96 TeV*, DØ Note 5436-CONF (2007). (`http://www-d0.fnal.gov/Run2Physics/WWW/results/prelim/NP/N56/`)

[11] V. Abazov *et al.* (DØ Collaboration), *Search for the lightest scalar top quark in events with two leptons in $p\bar{p}$ collisions at $\sqrt{s}$=1.96 TeV*, hep-ex/0707.2864 (2007).

[12] DØ Collaboration, *Measurement of the $t\bar{t}$ pair production cross section in $p\bar{p}$ collisions at $\sqrt{s}$=1.96 TeV in the lepton+jets final state using lifetime tagging on 900 pb^{-1} of DØ data*, DØ Note 5355-CONF (2007). (`http://www-d0.fnal.gov/Run2Physics/WWW/results/prelim/TOP/T43/`)

[13] T. Sjöstrand, L. Lönnblad, S. Mrenna, P. Skands, *PYTHIA 6.3: Physics and manual*, arXiv:hep-ph/0308153 (2003).

[14] M.L. Mangano *et al.*, *ALPGEN, a Generator for Hard Multiparton Processes in Hadronic Collisions*, JHEP **0307**, 001 (2003).

[15] S. Höche *et al.*, *Matching Parton Showers and Matrix Elements*, arXiv:hep-ph/0602031 (2006).

[16] E.E. Boos *et al.*, *Method for simulating electroweak top-quark production events in the NLO approximation: SingleTop event generator*, Phys. Atom. Nucl. **69**, 1317 (2006).

[17] S. Agostinelli *et al.* (GEANT4 Collaboration), *GEANT4: A simulation toolkit*, Nucl. Instrum. Meth. A **506**, 250 (2003).

[18] S. Snyder, *Measurement of the Top Quark Mass at DØ*, Doctoral Thesis, State University of New York at Stony Brook (1995).

[19] I. Bertram *et al.*, *A Recipe for constructing confidence limits*, Fermilab-TM-2104 (2000).

[20] T. Andeen *et al.* (DØ Collaboration), *The DØ experiment's integrated luminosity for Tevatron Run IIa*, Fermilab-TM-2365 (2007).

[21] It has been shown that the relative contributions of the heavy flavor samples $Wc\bar{c}$ and $Wb\bar{b}$ have to be scaled up by the factor of $k_{HF} = 1.17 \pm 0.18$ to model the data.

Appendix A: Control Plots

This appendix shows the data-MC agreement for selected control variables: p_T of the highest-p_T jet (leading jet), lepton p_T and missing transverse energy $\not\!\!E_T$. The variables are shown before and after b-tagging for events with four or more jets in both channels. The signal contribution is not included in the Monte Carlo distributions, but as an example the corresponding histograms for the 175/135 mass point are overlaid ten times enhanced.

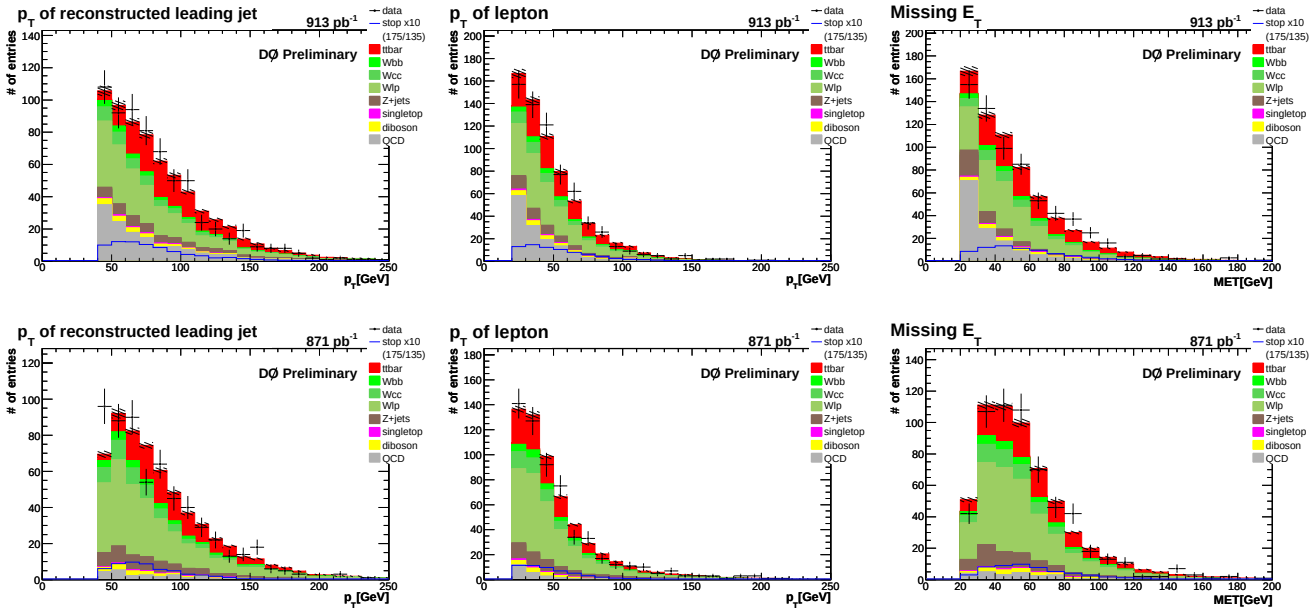

Figure 7: Data-MC agreement for ≥4 jets before b-tagging. Top: e+jets channel, bottom: μ+jets channel.

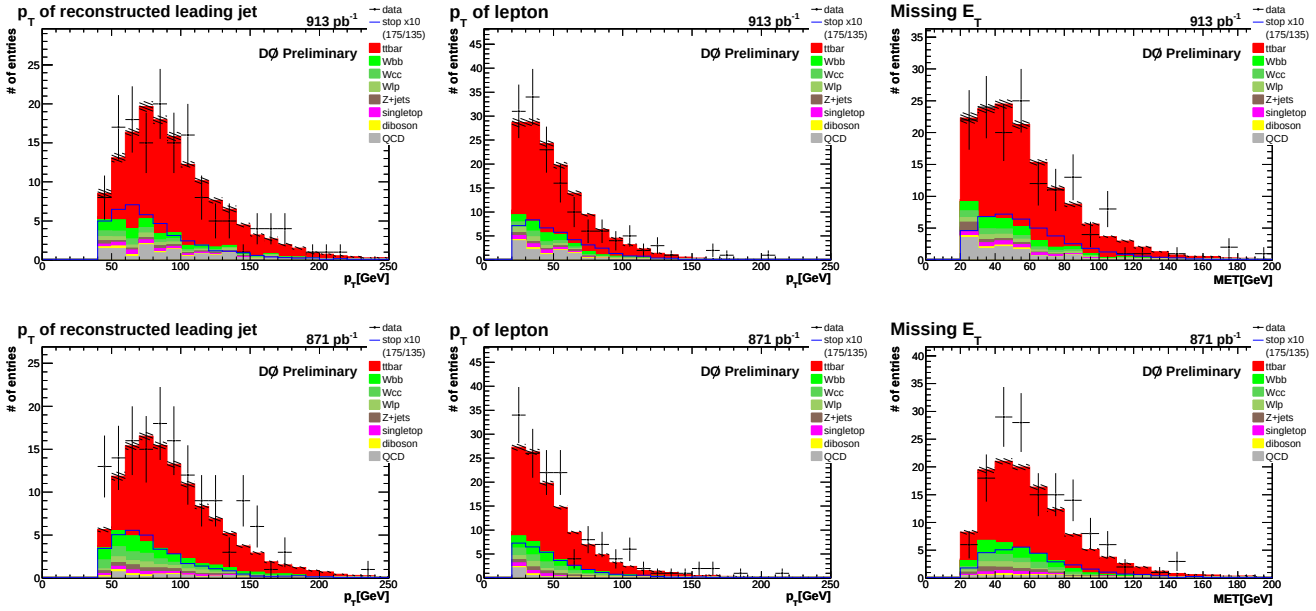

Figure 8: Data-MC agreement for ≥4 jets after b-tagging. Top: e+jets channel, bottom: μ+jets channel.

Appendix B: Likelihood Discriminant

In this appendix the likelihood discriminant for the Stop 175/135 mass point as well as the four input variables are shown. They appear both as comparison between the signal, the $t\bar{t}$ background and the W+jets samples and as data-MC comparisons. The data-MC comparison plots are shown in the signal bin with four or more jets after b-tagging and after HITFIT convergence. The signal contribution is not included in the Monte Carlo distributions, but as an example the corresponding histograms for the 175/135 mass point are overlaid ten times enhanced.

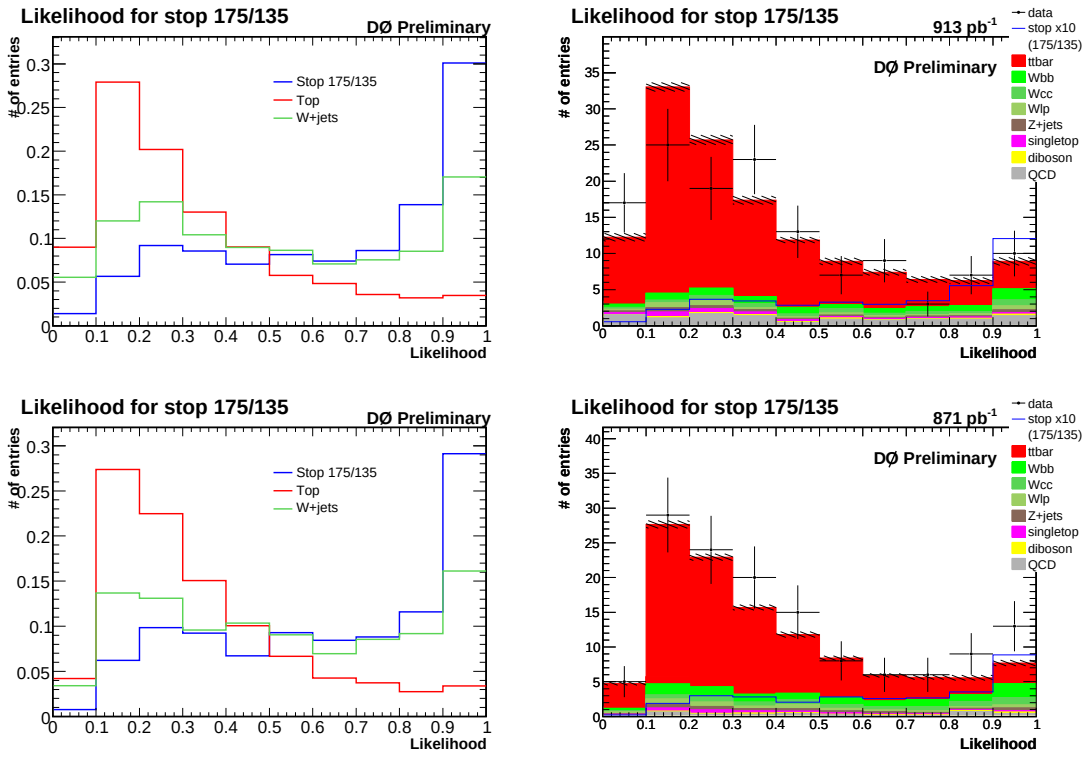

Figure 9: Likelihood discriminant for the Stop 175/135 mass point. In the data-MC comparison on the right the distribution for the 175/135 mass point is overlaid ten times enhanced. Top: e+jets channel, bottom: μ+jets channel.

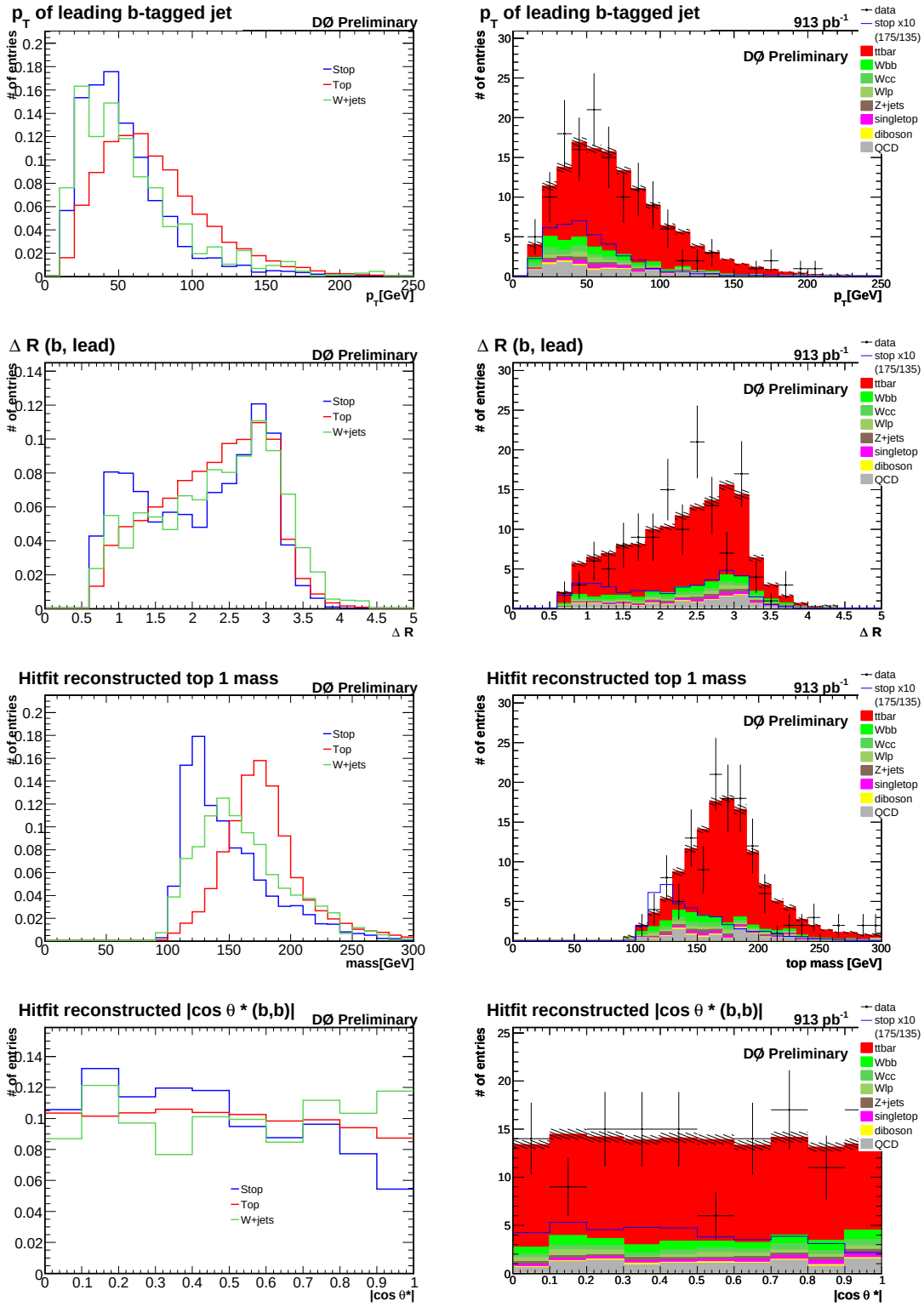

Figure 10: Input variables for the Stop 175/135 mass point in the e+jets channel. In the data-MC comparison on the right the distribution for the 175/135 mass point is overlaid ten times enhanced.

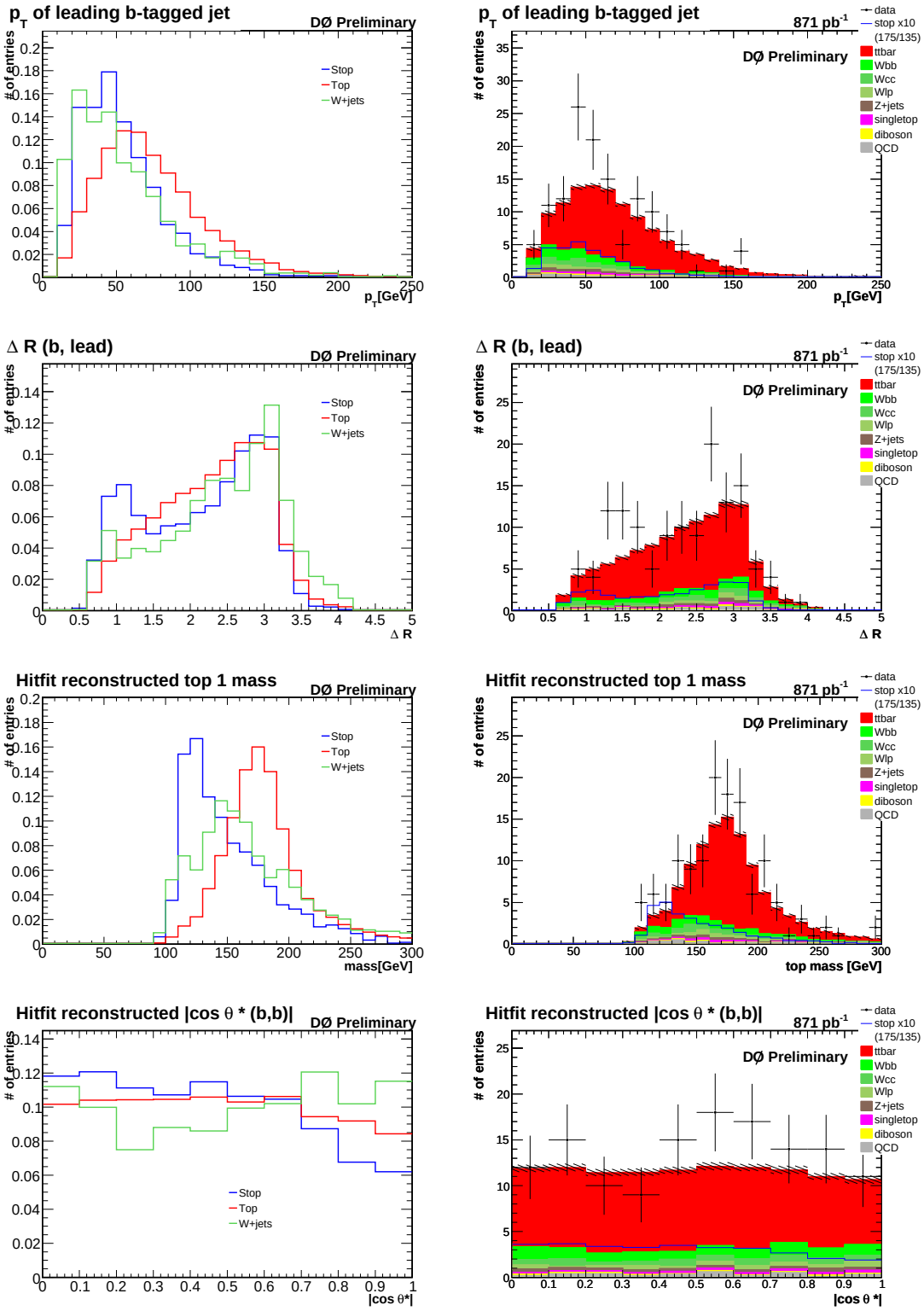

Figure 11: Input variables for the Stop 175/135 mass point in the μ+jets channel. In the data-MC comparison on the right the distribution for the 175/135 mass point is overlaid ten times enhanced.